Structure-property correlations of the heat-treated and friction-stir processed AA7075T7352

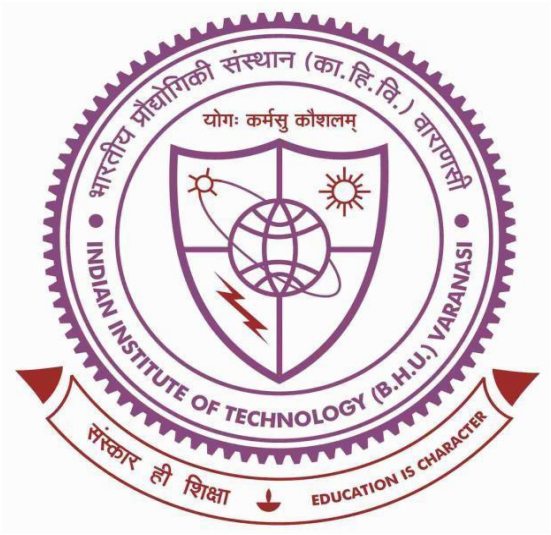

Thesis submitted in partial fulfillment for the Award of Degree

DOCTOR OF PHILOSOPHY

BY

ROOPCHAND TANDON

DEPARTMENT OF METALLURGICAL ENGINEERING
INDIAN INSTITUTE OF TECHNOLOGY
(BANARAS HINDU UNIVERSITY)
VARANASI–221005 INDIA

17141008 **2024**

Preface

Owing to high specific strength, good formability, and toughness, as well as improved fatigue and stress corrosion cracking (SCC) resistance, enhanced ballistic performances, and work-hardening exponent (n), the 7xxx series Al alloys are widely used in aerospace, armour, and automobile industries. The majority of strengthening in these arises due to precipitation. There is an inseparable relationship between the precipitation process and the mechanical properties. The precipitation process of such alloys depends on the Zn/ Mg ratio. For a higher Zn/ Mg ratio (≥2), the precipitation sequence is given as Supersaturated solid solution SSSS *(α)→GP-zones (coherent) → η' (semi-coherent) → η (in-coherent)*. Since its inception, heat treatments (T73, T7651, RRA, IA), alloying additions (Ag, Sn, Sc), and surface modification techniques, e.g., ultrasonic shot peening (USSP), laser shock peening (LSP), and friction stir processing (FSP) are given for improving the engineering performances. Such techniques strongly influence the micro-structural features along the processed zones and, therefore, the mechanical properties. Present work, therefore, shows structural property correlations of the heat-treated 7075 Al-alloy respective to T4, T6, T73, and T7352 tempers, as well as cold rolled alloys followed by the peak-aging (S.Q.+15%CR+P.A., denoted as TMP-1, S.Q.+ 30% CR+P.A., denoted as TMP-2, and S.Q.+45% CR+P.A., described as TMP-3), and friction stir processing of AA7075T7352 (1000 rpm) up to three passes. The AA7075T7352 was designed to obtain the high work hardening exponent (n) and high ultimate tensile strength to yield a strength ratio (UTS/ YS), which is a function of the dislocation structures. Therefore, dislocation structures of partially tensile deformed AA7075T7352 alloy were investigated, and the thesis has been organized into six chapters.

Chapter 01 gives a brief introduction and a description of the specific properties of the 7xxx Al-alloys. The techniques used for property enhancement and the development of age-hardenable Al-alloys are discussed. Yearwise introduction of the age-hardenable Al-alloy with specific properties and their applications are also illustrated. The knowledge gaps are identified after a successful literature review, and we have formulated certain objectives to address the knowledge gaps associated with the alloys, which are given below:

- Nature of precipitates in AA7075T7352. The size, morphology, and distribution of precipitates are illustrated
- Nucleation behaviors of the metastable *(GPzone, η)* and equilibrium *(η)* precipitate
- Hardening and flow behaviors study of under-aged (T4), peak-aged (T6), over-aged (T73), and T7352 tempered 7075 Al-alloy.
- To study the precipitation behaviours of the partially tensile deformed AA7075T7352.
- Correlations of dislocation structures with hardening performances of the AA7075T7352.
- Effect of thermo-mechanical processing on microstructure evolution and mechanical properties of AA7075T7352.
- Depth-wise microstructure evolution and texture study of friction stir processed AA7075T7352
- Variation of the microstructures and textures of the multi-pass friction stir processed AA7075T7352.

Chapter 02 Deals with the experimental methods and characterization techniques used for the structure-property correlation. The alloy used in the current investigation was procured from Deccan Smith Private Limited, India, whose chemical composition is in Table 1. The 7075 Al-alloy was given various heat treatments, for instance, under-ageing (T4), peak-ageing (T6), over-ageing (T73), and T7352. Further, the AA7075 was thermo-mechanically processed by solution

quenching (470 °C for 2 hours), followed by three different amounts of cold rolling (15%, 30%, 45%) and peak-aging at 120°C for 24 hours. The cold-rolled and peak-aged samples at 15%, 30%, and 45% are designated as TMP-1, TMP-2, and TMP-3, respectively.

Interrupted testing deformation (at 2%, 6%, and 10% tensile true strain) was given to study the dislocation behaviours. TEM samples are prepared from the gauge section of the partially deformed alloys. Dislocation structures are characterized with the help of weak-beam dark-field TEM imaging with the help of Tecnai G^2-20 TEM operated at 200kV. Weak beam conditions are obtained after suitable tilting of α and β. The excitation error "s" was maintained positive during imaging. The resultant dislocation structures are co-related with the mechanical properties. AA7075T7352 alloys are refined by friction stir processing. A suitable tool (6mm pin length with threading and 20mm shoulder diameter) is designed for processing (at 1000 rpm). A suitable tool (6 mm pin length with threading and 20 mm shoulder diameter) was designed to process the alloy (at 1000 rpm). The phases and precipitates are analysed with the help of X-ray diffraction (XRD) and transmission electron microscope (TEM). The residual stress and bulk texture measurement are also done using the HR-XRD (three-dimensional scanning: *Chi, Phi, Omega*). Micro-textures of heat-treated and FSP samples are studied with the help of electron-backscattered diffraction (*EBSD*).

Chapter 03 gives the effect of microstructure, texture, and mechanical behaviours of the heat-treated 7075 Al alloy. This is categorized into three major parts. Part I deals with the electron microscopy of precipitates in AA7075T7352 alloy. Part -II is related to the effect of partial tensile deformation on the precipitation and dislocation behaviours of the AA7075T7352. On the other hand, part III is attributed to microstructure evolution, texture characteristics, and flow behaviours of the aged (T4, T6, T73) 7075 aluminium alloy.

In part I, the alloy AA7075T7352 shows the formation of GPzone, η', and η precipitates randomly distributed throughout the α-Al. The nucleation of η' and η occurs by separated nucleation and in-situ nucleation mechanisms. The 6 to 7 small η' (rod-type) precipitates coalesce along 110 of α-Al and form larger precipitates. On the other hand, two differently oriented η precipitates along $1\bar{1}0$ and 110 of α-Al are coalesced at the interface by changing the lattices and form new η precipitates by changing the lattices, indicating the in-situ nucleation mechanisms assisted precipitation. Some of the η' and η precipitates form without coalescence, and these are freely nucleated, displaying the separated nucleation-assisted formation of precipitates. The d-spacing value of Al_3Zr dispersoid (1.43Å) is the same as that of 220 of α-Al (1.43Å). On the other hand, GPzone follows the 3rd-order lattice multiplicity concerning 220 of the α-Al. The GPzone has less interfacial energy (0.01-0.05J/m^2). Therefore, its nucleation occurs in the beginning. The η has high interfacial energy (0.4-1.0 J/m^2), and its nucleation occurs in the last stage. On the other hand, the interfacial energy of η' (0.1 to 0.3 J/m^2) is between the GPzone and η. Hence, nucleation occurs in the intermediate stage, and the alloy follows the precipitation sequence as of supersaturated solid solution (SSSS (α))- GPzones -η' -η. The dislocation entrapment in the interface of α-Al and η is another major observation. Satellite spots with 4-fold symmetry along 001 of α-Al form due to metastable precipitates. On the other hand, streaking along $1\bar{1}0$ of α-Al arises due to the formation of stacking fault type of homophase interface, which evolves during nucleation of the η precipitates.

In part II, Partial deformation for 2%, 6%, and 10% tensile true straining also changes the chemistry and size of precipitates. On 2% partial deformation (tensile true straining), GP zone *and η'* are partially dissolved. After 6% deformation, the GP zone is fully dissolved, but the η' and η are partially dissolved. Meanwhile, at 10%, the deformation formation of the GPzones is

accelerated. The dislocation re-arrangement occurs on account of the partial deformation. Dislocation loops and forest dislocation are observed on 2% tensile true-straining. Low and high-density Taylor lattice structures are seen for 6% partial deformation. On the other hand, low- and high-density dislocation cell structures are observed for 10% partial tensile deformation. Changes in significant reflection of XRD peaks illustrate the texture development on account of the partial deformation.

In part III, under-aged (T4) alloy does not form precipitates because room temperature ageing (30 °C for three days) is not enough for the decomposition of the supersaturated solid solution (SSSS). On the other hand, formation of the GP zone, η', and η are observed on T6 temper (peak-ageing) due to elevated temperature ageing (120 °C, for 24h), which is sufficient for decomposition. The grain boundary (η) precipitates are continuously distributed. In the over-aged (T73) condition, some amount of η' is survived, and the η precipitates are mainly formed as a result, the lattice parameter of α-Al is decreased. This also shows the thermally assisted dissolution of GPzones as the temperature of second-stage ageing (180°C for 30h) is well above its solidus temperature. The grain boundary η precipitates in the T73 condition are coarser than the T6 condition and discontinuously distributed. The grain boundary precipitates are coarser than the T6 temper and discontinuously distributed. The T7352 shows the formation of the GPzone in addition to the η' and η phases, as well as those of Al_2Cu, Al_2CuMg, and Al_3Zr dispersoids. Also, dislocation entrapment in the interface of η and α-Al is observed. The heat-treated alloys on T4, T6, and T73 tempers do not show significant differences in texture characteristics and present the evolution of Goss {011} <100> texture with nearly the same intensity (14.8xR). On the other hand, T7352 illustrates the evolution of the Goss {011} <100> texture with enhanced intensity (x24 R). Such enhancement on Goss {011} <100> texture creates a significant angle twist grain boundary

for the nearby grains, thereby increasing the crack resistance. The yield strength, YS (464±3 MPa), and ultimate tensile strength, UTS (480±7 MPa) of T6 temper, is higher than that of other conditions. Moreover, the UTS to YS ratio (1.14) is high for T7352 temper. The aged alloys on T4, T6, and T73 tempers follow the Swift ($\sigma = K(\varepsilon+\varepsilon_0)^n$) flow behaviour. On the other hand, T7352 temper depicts the best fittings with Ludwigson ($\sigma = K_1\varepsilon^{n1}+exp\ (K_2+n_2*\varepsilon)$) flow curve. However, fitting parameters are different due to variations in size, morphology, and distribution of precipitates. The T4 temper shows the ductile mode of failure. On the other hand, T6, T73, and T7352 depict mixed modes of ductile and brittle failures.

Chapter 04 discusses the microstructure evolution, texture, and mechanical properties of the thermo-mechanically processed AA7075T7352 alloy. Volume fractions of GPzone are more in the case of TMP-1. On the other hand, enhanced fractions of the η' and η are observed corresponding to TMP-2 and TMP-3 alternatively. The TMP-1 shows accelerated precipitation of GPzone. On the other hand, TMP-2 and TMP-3 display dislocation entrapment at the interface of α-Al and η precipitates, which provides the coupling effect between the dislocation-precipitates interface. The coupling intensity in TMP-3 is higher than in TMP-2, which improves the strength-ductility trade-off and those of stress corrosion cracking (SCC) performances. The bulk-textures and micro-texture display similar features. However, differences in intensity arise due to variations in the scanning area. Evolution of the Goss {011} <100> is noticed in the peak-aged (T6) condition with less intensity (x14.8). On the other hand, presence of the Cu {112} <111>, and S {123} <634> textures are observed including the Goss {011} <100> texture after TMP. The intensity of Goss {011} <100> texture increases while increasing the amount of deformation obtained to be 20, 25 and 27 times random, respectively, for the TMP-1, TMP-2, and TMP-3. The alloy AA7075 on SQ, T6 and TMP-1 conditions follow the Swift flow behaviour, but their flow curve parameters are

different due to variations in the precipitates' size, shape and morphology. On the other hand, TMP-2 and TMP-3 show the best fittings with Ludwigson $(\sigma = K_1\varepsilon^{n1} + exp\ (K_2 + n_2 * \varepsilon))$ flow behaviours, which is supported by two different intensities of coupling effect of dislocation and precipitates that also changes the hardening parameters in two-different strain regimes.

Chapter 05 illustrates the evolution of the microstructures and texture of friction stir processed AA7075T7352 and their effects on tensile properties, hardness, and residual stress.

The GPzone is fully dissolved after 1pass FSP. On the other hand, *η' and* Al_2CuMg phases are partially dissolved, and the growth of the $Al_2Cu\ (\theta)$ phase is observed. The dissolution occurs by the combined effect of dislocation-shear as well as those of friction stir-assisted thermal effect. The Al23Cu Fe4 intermetallic formation is observed due to pipe-diffusion and the dislocation sweeping mechanisms. The *GPzone and η'* phases both are dissolved after 2pass FSP. On the other hand, re-precipitation of *GPzone* is observed with different chemistry but the same crystal structures after three passes. Precipitation of the *η' and η* are observed, but size and volume fractions of η' are reduced, but the size of the η remains unchanged. The η precipitates from grain boundaries are dissolved after FSP. Such dissolutions and coarsening and growth of precipitates following FSP would likely help gain improved mechanical properties. The grain boundary precipitates are also dissolved, followed by the FSP. After 1pass FSP, the NZ shows dynamically recrystallized but equi-axed refined grains. The TMAZ displays slightly elongated grains, with coarse grains in HAZ. On the other hand, base-metal (BM) remains unaffected after FSP. Similar microstructures also evolved after two and three passes of FSP. The top of NZ after 1pass FSP shows dislocation peening and the parallel array of dislocation structures. The middle portion displays a dislocation network and a parallel array of dislocation structures. The bottom region shows sub-grain formation and dislocation cell-type structures.

The FSP randomizes texture components. The texture intensity of Goss texture {011} <100> for base metals is 24 times random. After 1 and 2 passes of FSP, texture intensity decreases to 2.5 times random, and 1.6 times random, respectively. At the end of 3pass FSP, the texture intensity becomes 2.1 times random. The Goss {011} <100>, Rotated goss {110} <110>, Rotated cube {001} <110>, and S {123} <634> textures are another noteworthy feature after FSP. The grain size of base metals (BM) or as-received (AR) alloy is 54±3 μm. One order of magnitude in grain refinement is 3.8±0.5 μm after one pass of FSP. On 2pass, the grain size becomes 3.5±0.6 μm. Moreover, at the end of 3 passes, the grain size further reduces to 2.6±0.4 μm. The low-angle grain boundary fraction (LAGBF) and high-angle grain boundary fraction (HAGBF) of as-received (AR) alloy are 85% and 15%, respectively. The HAGBF after 1pass FSP increases to 49% due to dynamic recrystallization. After 2pass FSP, the HAGBF slightly reduced to 47%, which further decreased to 30% after 3pass FSP, but it was more than the AR condition. The KAM value of BM metal is 0.52°, which increases to 0.56° after 1pass FSP and thereafter decreases to 0.45° for 2pass FSP. The KAM value further increases to 0.65° for 3pass FSP. The co-incident site lattice (CSL) boundary fractions of AR alloy's Σ3, Σ5, and Σ9 boundaries are 0.75, 0.19 and 0.35, respectively. After 1pass FSP, CSL boundary fractions of Σ3, Σ5, and Σ9 increase to 1.25, 0.65, and 0.55. The respective boundary fractions of Σ3, Σ5, and Σ9 after two passes FSP further increase to 1.35, 0.95, and 0.85. The CSL boundary fractions of Σ3, Σ5, and Σ9 slightly decrease to 1.0, 0.65, and 0.55 after 3 passes of FSP.

Friction stir processing (FSP) further changes the nature of residual stress (RS). After one pass FSP, the RS in NZ and HAZ are -132±3 MPa and -110±6 MPa, respectively. On the other hand, RS in the base metal or unaffected region is less compressive at -96±8 MPa. On two-pass FSP, the compressive nature of RS increases to -153±7 MPa, due to further dynamic re-crystallization-

assisted grain refinement. After three passes of FSP, residual stress slightly decreases to -148±4 MPa due to re-precipitation of GPzone. The average hardness of BM is 133±4 Hv. On 1pass FSP, the average hardness of NZ increases to 155±4 Hv. On 2pass FSP, average hardness in NZ further enhances to 193±7 Hv. On the other hand, average hardness decreases to180±5 Hv in NZ for the three passes of FSP.

After one pass FSP, the strength decreases due to the dissolution of precipitates. Thereby, ductility increases, but significant enhancement in ductility is observed. On 2pass FSP, the strength decreases due to complete dissolution of GPzone and partial dissolution of η', which further enhances the ductility compared to 1pass FSP. The strength further decreases due to the dissolution of precipitates. On the other hand, ductility decreases due to re-precipitation of the GPzone with different chemistry but the same crystal structures. After FSP (1pass, 2pass, and 3pass), the alloy depicts the Swift flow behaviour, but pre-strain (ε0) and work hardening exponent(n) are different due to changes in the size and chemistry of precipitates.

Chapter 06 Gives significant conclusions drawn from the current investigation. This also consists of suggestions for future work, which are given at the end of the thesis.

Among all the heat-treated Al-alloy, T7352 performs best due to the evolution of deformation textures, compressive residual stress, complex dislocation structures, Ludwigson-fitted flow curve behaviour, and improved ductility. Thermo-mechanical processing improves the strength ductility trade-off due to the coupling effect of dislocation and precipitates, and the evolution of deformation textures is noticed. The GPzone, η' precipitates are separately nucleated. On the other hand, nucleation of η occurs by in-situ nucleation mechanisms which follow the precipitation sequence as SSSS(α)→GPzones (GP-I&GP-II) →η' →η. Texture and grain size do not change during T4,

T6, and T73 tempers. However, significant grain size reduction and increased low-angle grain boundary fractions are observed at T7352 temples. Among all the heat-treated alloys, T7352 display Ludwigson fitting. However, T4, T6, and T73 show the best fittings with the Swift flow curve. Partial deformation displays the dissolution of GPzone at a lower amount of deformation and re-precipitation with different chemistry, but the same crystal structures are noticed at T7352. The dislocation re-arrangement occurs during the partial tensile deformation, and dislocation entrapment will enhance the corrosion performance.

The gradient of the microstructure and hardness is observed after FSP due to the microstructural gradient throughout the processed regions. Increased high-angle grain boundary fraction, High KAM, and grain size reduction show the dynamic re-crystallized grain structures. Dislocation peening and recovered microstructure are observed at the top, with parallel dislocations in the middle. In contrast, cellular dislocation and unaffected regions are noticed at the bottom of the processed alloy. Increased compressive residual stress and formation of the dynamically re-crystallized refined grains enhance the performances of the alloy. However, texture intensity decreases due to thermal softening. GPzones are completely dissolved up to 2-pass. Thereafter, re-precipitation of it occurs at the 3-pass FSP. The compressive nature of residual stress increases while increasing the passes to 3. The nugget zone displays the highest compressive nature and thereafter decreases moving towards the base metal (BM). Such observations would likely be helpful for improving the SCC as well as the other mechanical performances.